USGS Award Number 05HQGR0072

Shallow Shear Wave Velocity Structure of the Charleston Historical District, South Carolina: Comparison of Surficial Methods and Borehole Results

Final Report to the US Geological Survey by:
Steven C. Jaume and Norman S. Levine
Department of Geology and Environmental Geosciences
College of Charleston
66 George Street
Charleston, SC 29424
Telephone: (843) 953-1802
FAX: (843) 953-5446
Email: jaumes@cofc.edu

Abstract

Surficial seismic data was collected at 21 sites in the greater Charleston, South Carolina region where shear wave velocity information from seismic cone penetrometer (SCPT) boreholes was available. Shallow shear wave velocity structure was characterized using shear wave refraction (6 sites) and an ambient seismic noise (refraction microtremor – ReMi) technique (21 sites) and compared to the SCPT results. It was determined that characterizing the shallow compressional wave velocity structure (water table depth) is required for accurate ReMi results. ReMi and shear wave refraction velocities compare well at 4 of 6 sites where both are available. SCPT and ReMi shear wave velocities compare well over depth ranges where SCPT data is available; however, most SCPT boreholes were found not to reach near 30 meters depth. V_{S30} estimates using the ReMi technique are generally equal to or larger than those using the SCPT data (assuming the deepest velocities go to 30 meters) alone. Results also suggest that V_{S30} is weakly correlated with age of the surficial geologic units, being generally faster in older sediments. A WebGIS product has been produced to disseminate seismic and borehole data collected or used as part of this project, plus other data useful for analyzing seismic hazard in the greater Charleston region.

Introduction

The greater Charleston, South Carolina region was severely damaged by the largest earthquake in the southeastern United States, the M = 6.9-7.3 earthquake of August 31, 1886 (Johnston, 1996; Bakun and Hopper, 2004). Persistent low-level seismicity combined with paleoliquefaction evidence suggesting a repeat time of 500-600 years (Talwani and Schaeffer, 2001) is reflected in the Charleston, SC region having the second highest seismic hazard east of the Rocky Mountains (Frankel et al., 2002). Earthquake ground motion at a particular location is strongly influenced by shallow geologic structure modifying the incoming seismic wave motion. Robinson and Talwani (1983) found that both building construction (brick versus wood frame) and site conditions (made versus solid ground) played a role in determining damage distribution during the 1886 earthquake. Determining the shear wave velocity structure of a site has

proven to be an effective input into predicting how these "site effects" influence the actual ground motion (Reference).

Recovering well-constrained shear wave velocity information has most often required relatively time consuming and expensive drilling and logging of boreholes. Our research focused upon collecting and interpreting surficial seismic data for shear wave velocity structure. In particular, we collected ambient seismic noise data and used a new technique termed "Refraction Microtremor" or ReMi (Louie, 2001) to determine shear wave velocity structure at 21 sites where Seismic Cone Penetration Test (SCPT, i.e., borehole) data already exist (Figure 1). The main objective of our study was to determine if the ReMi technique provides an adequate substitute for the SCPT method and the most effective field experiment methodology for utilizing the ReMi technique in the geologic conditions of the greater Charleston region.

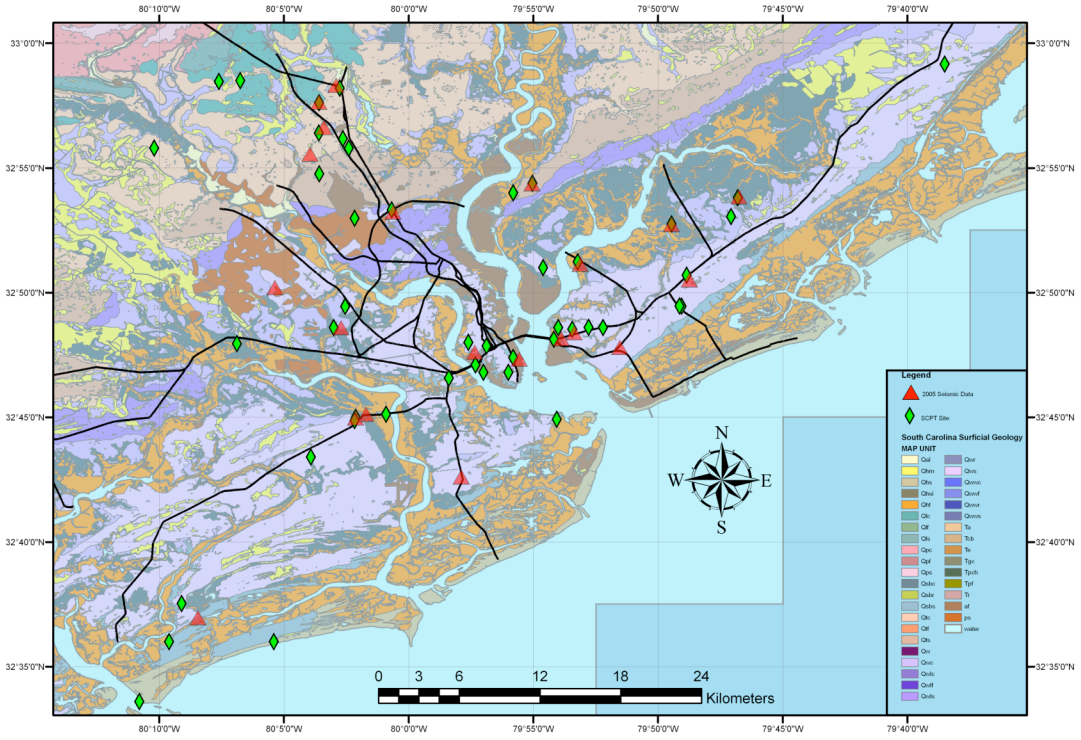

Figure 1: Map of study area showing surface geology, seismic data collections sites (red triangles) and SCPT boreholes (green diamonds) from the database of Chapman et al. (2003). Note that all seismic data collection was conducted near SCPT sites but several either did not have locations in the Chapman et al. (2003) database or were mislocated.

Investigations Undertaken

We selected sites for the seismic data collection based a database of SCPT results and locations reported in a previous NEHRP study by Chapman et al. (2003). M.

Chapman also shared additional notes describing the site locations. The latitude and longitude information for the SCPT sites was incorporated into a GIS product that included relatively recent (1999) aerial photographs and a road network database. Based upon this initial review it was apparent that some latitude and longitude information was incorrect; i.e., sites documented as being next to building sites were located in the midst of marshes, etc. Consultation with M. Chapman revealed that his team had difficulty in remotely locating some sites from field report maps made when the original SCPT work was done (Note: Due to the rapid growth of the Charleston metropolitan area many new streets and structures do not appear on publicly available geographic databases). Therefore we also visited the local offices of two local firms who conducted most of the original SCPT work (S&ME, Inc. and WPC Engineering, Environmental and Construction Services) and were graciously allowed to photocopy maps from the field reports. With this information we were able to more accurately locate some SCPT boreholes and even determine the location of three SCPT sites that Chapman et al. (2003) were unable to find (Figure 1).

Sites were chosen for seismic data collection primarily on the availability of space to deploy a seismic refraction line of at least 60 meters in length. This minimum length was chosen as the approximate length needed to define the shear wave velocity structure to a depth of 30 meters using the ReMi technique. In practice we deployed geophones along lines ranging from 69 to 184 meters (i.e., 24 geophones spaced at 3 to 8 meters). At all 21 sites we collected P-wave refraction data using a sledgehammer source and vertical 4.5 Hz geophones. J. Louie (pers,. comm.) has noted that using a P-velocity model as a constraint improves the shear wave velocity model interpreted using the ReMi technique when the Poisson's ratio of the sedimentary material is significantly greater than 0.25 (i.e., a P vs. S velocity ratio >> 2). These were reversed profiles at 20 sites; due to equipment problems we did not collect a reversed profile at one site (see Table 1 for details of data collected at each site). We also collected shear wave refraction data at seven sites (Table 1) using horizontal 4.5 Hz geophones with the recording axis oriented perpendicular to the long dimension of the array (SH-orientation). The shear wave source consisted of a block of wood pinned beneath a vehicle tire and struck horizontally by a sledgehammer. Six of the seven shear wave refraction lines are reversed profiles. At all 21 sites we recorded six or twelve 30-second long ambient seismic noise profiles using both the vertical and horizontal geophones; in this case the recording axis of the horizontal geophones were oriented parallel to the long dimension of the array (SV-orientation). In all of the above cases we deployed the geophones on the ground surface; i.e., spiked as firmly as possible into the soil. Given our goal of accessing the ReMi technique as a means of rapid site assessment we did not bury the geophones. It was noted that at several sites extremely loose or compact soil did allow for good geophone coupling. At 5 sites (Table 1) we also deployed geophones on a hard surface (asphalt or concrete) by detaching the spikes and placing the geophones upon common red bricks. We collected only ambient noise data in this manner. During our SCPT site location investigation phase we noted that at several SCPT sites (primarily in downtown Charleston) there was no available space to deploy geophones on a soil surface. Thus we wanted to have some ambient noise data collected on a hard surface to compare with data collected using geophones coupled to the soil, to determine if the ReMi technique performs well under these conditions.

Table 1: Locations of field sites and data collected during summer 2005. Site codes allow reference to SCPT data (S = S&ME; W = WPC) in the database of Chapman et al. (2003). R = reversed profile; NR = non-reversed profile; refrac = refraction line; Vert = ambient noise using vertical geophones; Horiz = ambient noise using horizontal geophones; (soil) = geophones spiked into ground; (brick) = de-spiked geophones placed on bricks; numbers represent number of 30 second ambient noise samples taken at each site.

Site Code	Latitude	Longitude	P refrac	S refrac	Vert (soil)	Vert (brick)	Horiz (soil)	Horiz (brick)
DNV3	32.8873	-80.0104	R		6		6	
DNV4	32.8524	-79.8853	R		6	6	6	
S99140	32.9721	-80.0485	R		6		6	
S99526	32.7521	-80.0285	R		6		6	
S01039	32.7936	-79.9558	R	R	6		6	
S01469	32.9438	-80.0566	R	R	6	6	6	
S01772	32.8026	-79.8979	R		6		6	
S02105	32.789	-79.926	R	R	6		6	
S02290	32.81	-80.0451	R		6	6	6	6
W01122	32.7968	-79.8588	R		6		6	
W01187	32.879	-79.8242	R		6		6	
W01239	32.8419	-79.8123	R	NR	6		6	
W01243	32.8369	-80.0893	R	R	6	6	6	6
W01252	32.8974	-79.7792	R	R	12	6	12	6
W01277	32.8066	-79.8893	R		6		6	
W01317	32.7102	-79.9648	R		6		6	
W02044	32.7497	-80.0353	R	R	6		6	
W02059	32.926	-80.0659	R		6		6	
W02073	32.9608	-80.0599	R		6		6	
W02096	32.6161	-80.1408	R		6		6	
W02104	32.9061	-79.9174	NR		6		6	

Data Processing

All seismic data were originally collected in SEG-2 format. We converted this data to SEG-Y format to allow for more flexibility in analysis and interpretation. Both the original SEG-2 data files and the converted SEG-Y files, together with a file describing relevant field parameters, can be accessed via the Charleston Seismic Hazard Consortium (CSHACe) WebGIS (http://maps.cofc.edu/website/cshacegis/viewer.htm). Selecting a ReMi site (remi_sites_jaume database) provides a link to a zip file containing the data files noted above.

P- and S-refraction data were interpreted by picking first arrivals and estimating velocities along linear first arrival segments. In most cases the raw field data were bandpass filtered to enhance clarity of the first arrival before picking. First arrival picks were exported into MS Excel and interpreted using slope and intercept for to produce a simple one-dimensional layered velocity structure. In a number of cases there are apparent dipping layers in the shallow velocity structure; we produced an equivalent one-dimensional structure by determining the true velocity of the lower layer and using the average depth of that layer boundary.

During the interpretation of the ambient seismic noise data (see next paragraph) it became apparent that the shallow P-velocity, in particular the depth of a large velocity increase at the top of the local water table, was an important constraint in modeling ambient seismic noise for shear wave velocity structure. Thus we interpreted all P-refraction data in terms of a two layered (unsaturated/saturated zone) model. Deeper, faster layers could be imaged in several refraction lines; however we found that including a more detailed P-velocity model in the ReMi modeling did not modify the results. We also interpreted the S-refraction data to produce one-dimensional layered velocity structures; in this case using as many layers as needed to adequately fit the first arrival data. Table 2 gives the resulting 1D P-velocity and Table 3 the S-velocity models. Note that we did not interpret the unreversed P- and S-refraction profiles.

Table 2: P-wave velocity structure at 20 sites where reversed refraction profile data was collected.

Site Code	Layer 1 (m/sec)	Boundary (meters)	Layer 2 (m/sec)
DNV3	287	1.49	1646
DNV4	238	2.73	1486
S99140	354	4.48	1620
S99526	321	2.03	1566
S01039	271	2.17	1568
S01469	309	3.01	1657
S01772	178	1.38	1484
S02105	223	4.78	1402
S02290	250	4.49	1456
W01122	267	3.31	1676
W01187	273	1.32	1560
W01239	260	1.71	1550
W01243	392	2.21	1651
W01252	342	2.08	1624
W01277	241	1.70	1589
W01317	226	1.99	1675
W02044	298	3.46	1616
W02059	485	3.11	1507
W02073	381	1.87	1686
W02096	246	1.71	1522

Table 3: S-wave velocity structure at 6 sites where reversed refraction profile data was collected.

Site Code	Layer 1 (m/sec)	Boundary 1 (meters)	Layer 2 (m/sec)	Boundary 2 (meters)	Layer 3 (m/sec)
S01039	178	13.77	458		
S01469	257	12.90	501		
W01239	162	7.22	234	458	31.30
W01243	209	4.70	525		
W01252	232	13.91	353	496	21.58
W02044	199	14.28	497		

Ambient seismic noise data were interpreted using SeisOpt ReMi™. The seismic traces are converted into p-tau (slowness-intercept time) space and a Fast Fourier Transform is applied to the tau domain to create a p-f (slowness-frequency) image of the

ambient seismic energy (see Louie, 2001 for details). The p-f image is then interpreted in terms of a Rayleigh dispersion curve, where an increase in spectral energy at large slowness (slowest velocity) is interpreted as Rayleigh waves traveling parallel to the line of sensors (Figure 2). A second module allows one to interpret the resulting Rayleigh dispersion curve in terms of a layered shear wave velocity structure based upon an algorithm by Saito (1979; Figure 3). This module allows one to adjust both V_p and V_s of a layered structure, plus the density. For our interpretations, we left the density at its default value of 2.0 g/cm^3. We constructed ambient noise derived shear wave velocity models for each site in two ways: 1) by simply adjusting shear velocities (assuming a V_p/ V_s ratio of 1.73) and layer thicknesses until we matched the Rayleigh dispersion picks, and 2) first fixing the V_p structure based upon the refraction results and then adjusting shear wave velocities only. Figure 4 shows the difference in the resulting velocity models for site DNV4 compared to SCPT velocities at the same site.

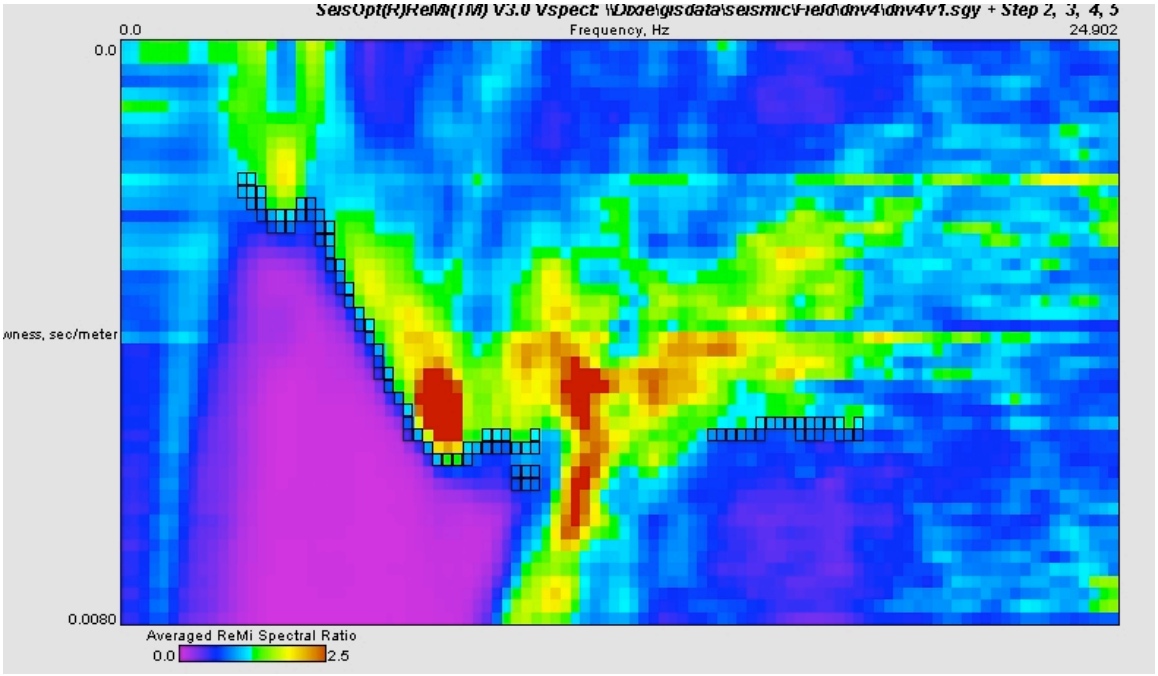

Figure 2: p-f image from ambient seismic noise collected at site DNV4. The lower boundary between p-f space with little or no spectral energy (violet/blue) and increased spectral energy (green/yellow/red) is picked as the Rayleigh dispersion curve (black boxes). The band of high spectral energy emerging from the center bottom of the image represents aliasing. See Louie (2001) for more details.

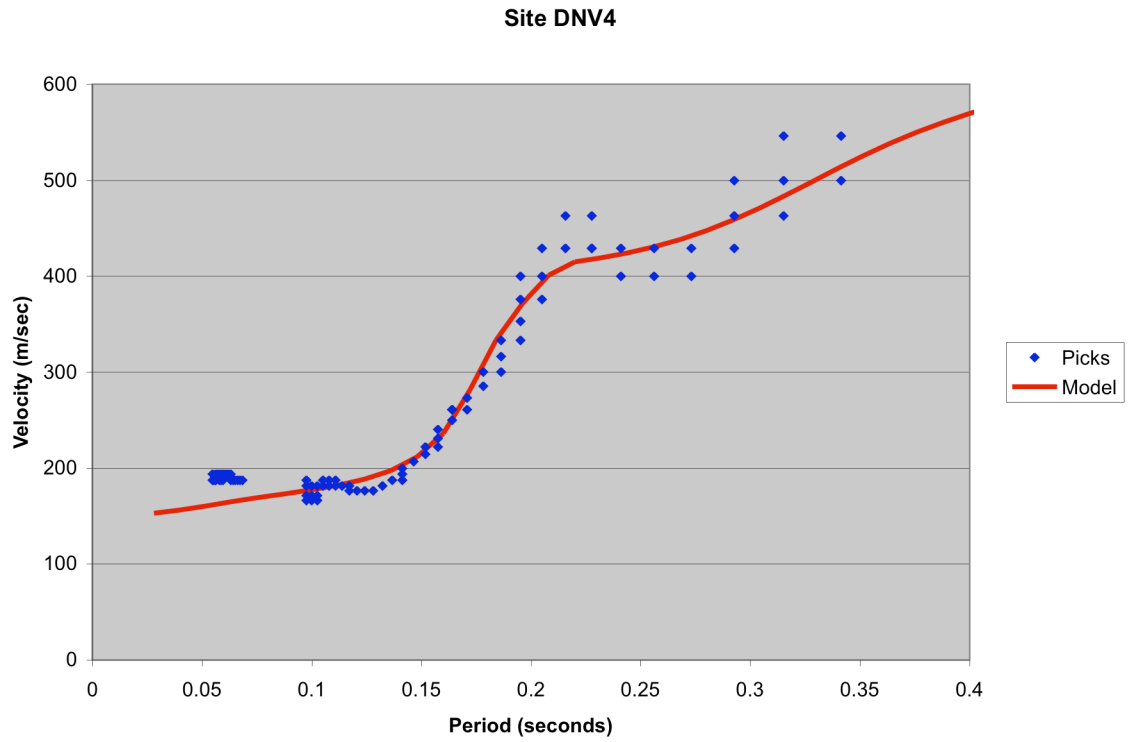

Figure 3: Modeled Rayleigh dispersion picks for site DNV4 (from Figure 2).

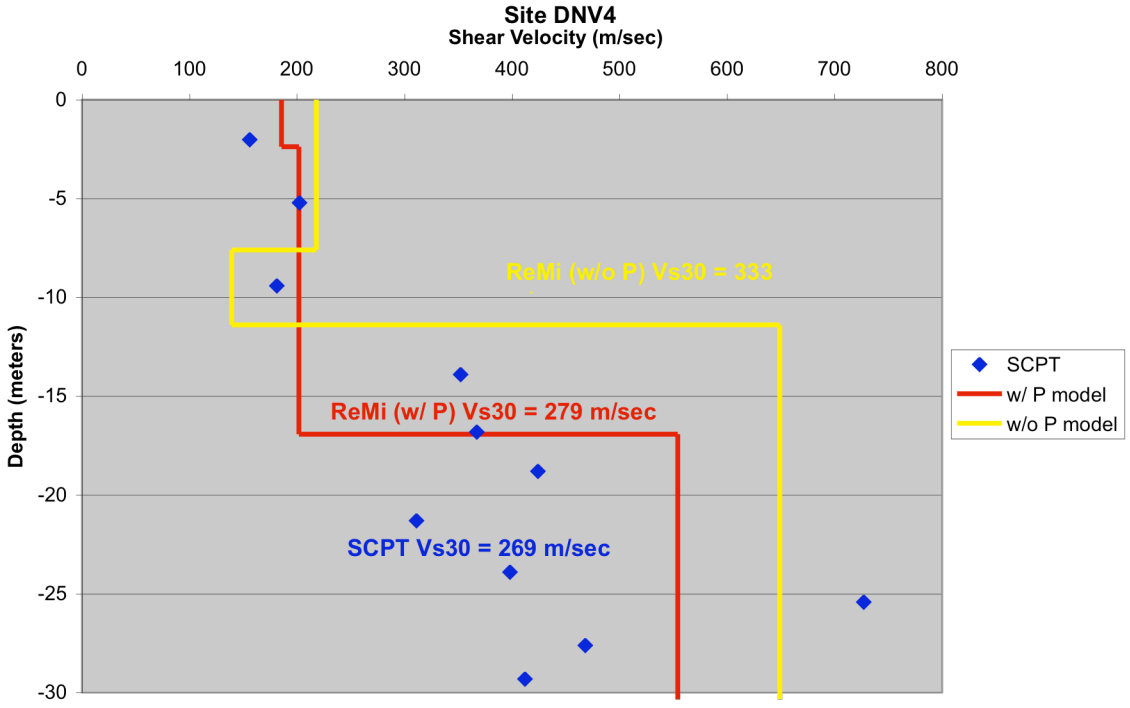

Figure 4: V_s structure at site DNV4 from SCPT data and modeling of refraction microtremor data with and without the P-velocity model constraint.

Results

Refraction Compressional Velocities

We found compressional velocities very similar to those of Odum et al (2003) for their sites in and near Charleston. The shallow soil V_p ranged from 178 up to 485 m/sec. V_p increased to near 1500 m/sec or more at depths ranging from 1.3 to 4.8 meters, which we interpret as the depth to the local water table. A maximum apparent V_p of 2780 m/sec was encountered at a depth of 14.6 meters at site W01243 (not on shown in Table 2).

Refraction Shear Velocities

Surficial V_s ranged from 178 to 257 m/sec. V_p/ V_s ratios for the soil above the water table at these sites ranged from 1.20 up to 1.88, averaging 1.53. However, in all cases V_p jumps to ~1500 m/sec or faster at very shallow depths and V_p/ V_s ratios just below the water table range from 6.45 to 9.57. At all depths resolved by the refraction data the V_p/ V_s ratio remained > 3. A maximum refraction-derived V_s of 525 m/sec was recovered at a depth of 5 meters. V_{S30} estimates using the refraction results range from 211 to 424 m/sec. These results are also comparable to that of Odum et al. (2003).

Ambient Noise Shear Velocities

Six to twelve sets of 30-second long records of ambient noise data were collected at each site (Table 1). We examined the individual p-f images from each set, selecting those that gave the clearest image (i.e., sharp break between purple - no seismic energy - and warmer colors representing seismic energy arriving in that p-f band) across the widest range of frequencies. In 11 of 21 cases we found that extending the high frequency cut-off of the p-f image to 35 Hz (from the default of 25 Hz) allowed us to better resolve V_s of the shallowest layer (Figure 5). We combined selected individual images into a final image from which we picked the Rayleigh dispersion values (Figure 3). At 16 sites vertical sensors spiked into the ground yielded data that produced the clearest p-f image, at 3 sites there was little difference between vertical and horizontal sensors spiked into the ground, at one site the horizontal sensors spiked into the ground yielded the best p-f image and at one site vertical sensors mounted on bricks on a sidewalk yielded the best p-f image. In general, we found that using vertical sensors for ambient noise recording yielded better results.

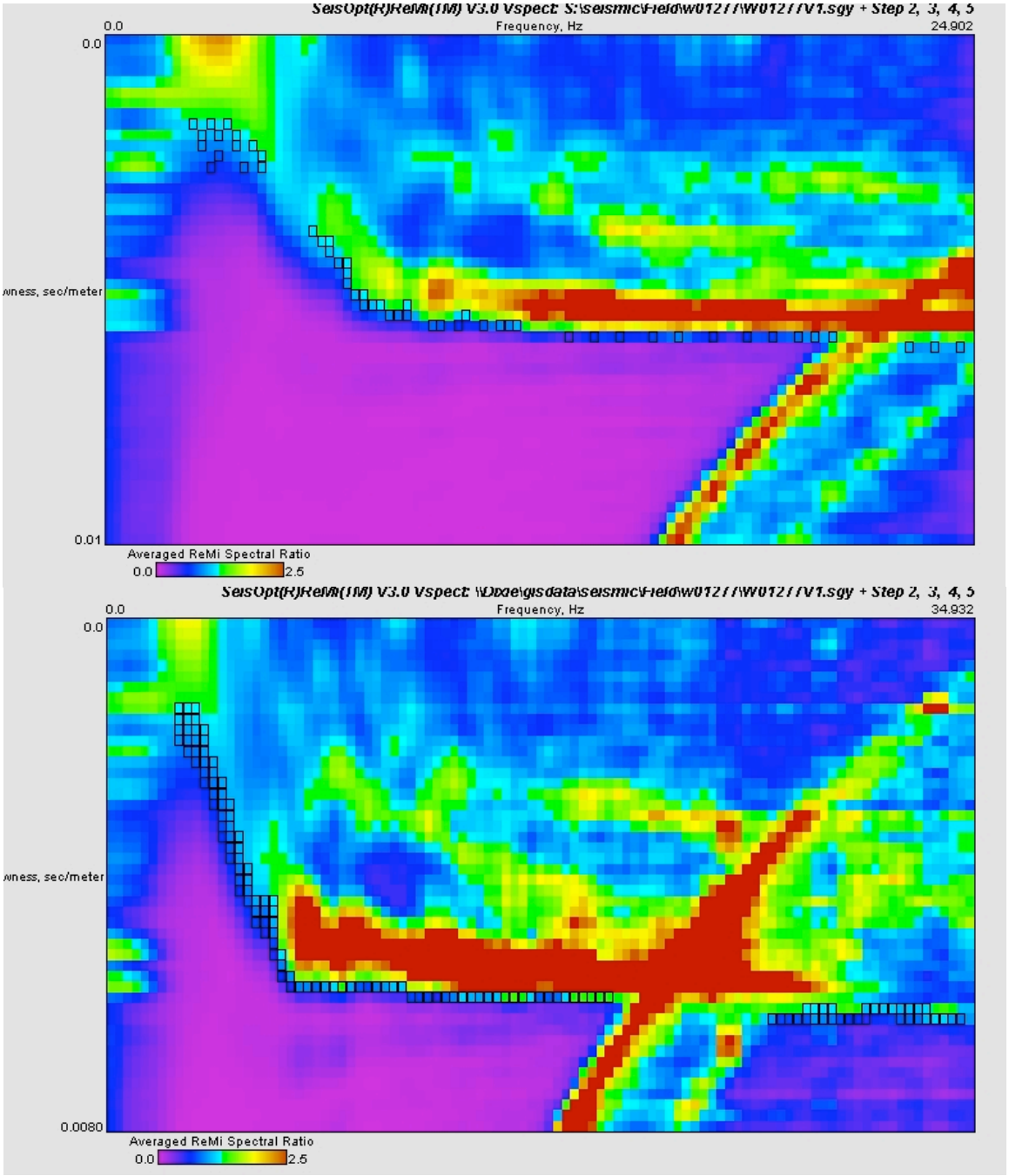

Figure 5: p-f images with Rayleigh dispersion picks for site W01277 using the default high frequency cutoff of 25 Hz (top) and extending it out to 35 Hz (bottom – note change in slowness axis also). In many cases the Rayleigh dispersion curve could be extended to frequencies above the aliasing band, leading to better velocity resolution of the shallowest layer.

As noted above, we constructed V_s models both with and without a V_p model constraint. We found that V_s structures derived in these two fashions were systematically different. In general, the depth to first major velocity increase was deeper and the velocity of the lower layer was reduced (Figure 4) when the V_p model constraint was

used. This results in a systematic decrease in the V_{S30} at each site if the V_p model constraint is used (Figure 4). We model this systematic decrease using both a constant and a linear fit (Figure 6). Our best-fit equations are (rms = root mean square misfit):

1) V_{S30} (P model) = V_{S30} (no P model) - 31.9 m/sec; rms = 4.56
2) V_{S30} (P model) = 0.820918V_{S30} (no P model) + 26.02 m/sec; rms = 3.94

We have a slight preference for using Equation 2 in the case where no P velocity model is available to constrain the Rayleigh dispersion modeling based on the lower rms misfit and the apparent slope on Figure 6 suggesting the misfit increases with V_{S30}. Table 4 shows the V_{S30} values at the ReMi 21 sites.

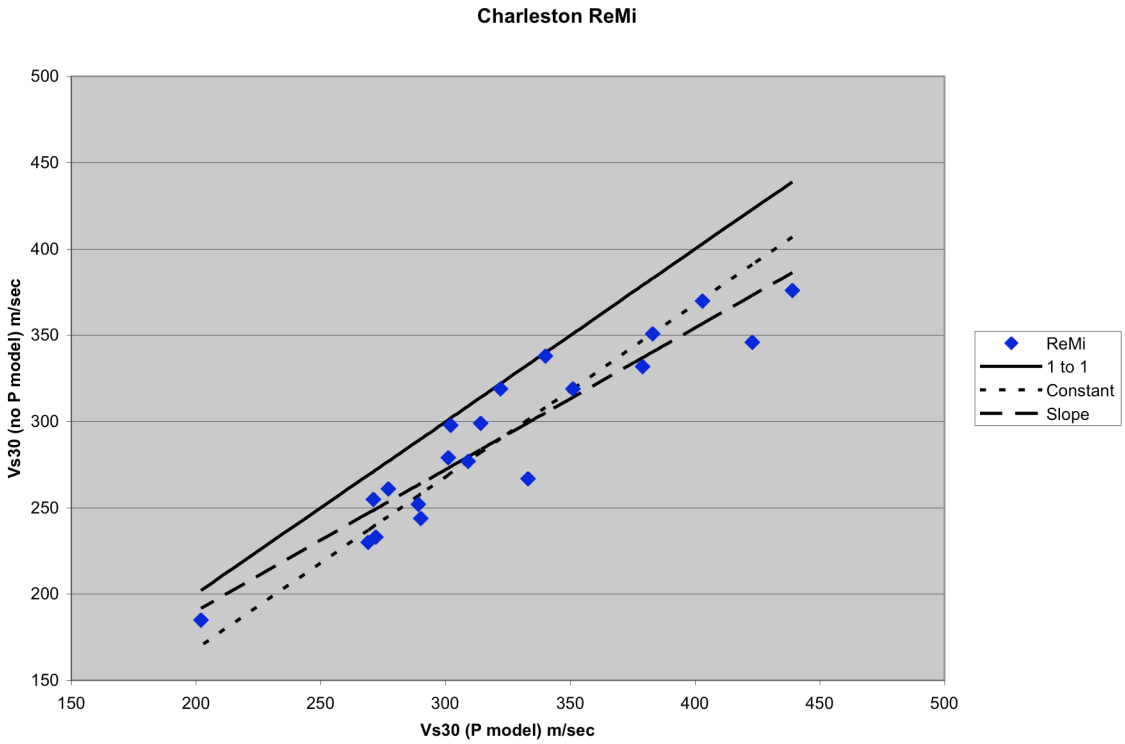

Figure 6: Comparison of ReMi V_{S30} at 20 sites where a P-velocity model was also available. V_{S30} is systematically lower when the P model constraint was used. A 1 to 1 line, Equation (1) and Equation (2) are also shown.

Table 4: V_{S30} estimated using the ReMi technique at study sites in the Charleston region. *ReMi V_{S30} at W02104 was estimated by assuming a P-velocity structure for the site; V_{S30} estimated using Equations 1 and 2 are shown in parentheses for comparison.

Site Code	V_{S30} (m/sec)
DNV3	371
DNV4	279
S99140	332
S99526	280
S01039	298
S01469	319
S01772	308
S02105	185
S02290	327
W01122	267
W01187	244
W01239	231
W01243	346
W01252	231
W01277	249
W01317	318
W02044	277
W02059	299
W02073	370
W02096	279
W02104*	241 (231/242)

Refraction versus ReMi V_s Models

Refraction and ReMi V_s models compare well both in structure and V_{S30} at four of the six sites where shear wave refraction data was collected (Figure 7 – example for site W01239). At the two sites where the match was poor the ReMi V_{S30} was consistently lower than the refraction V_{S30}; at one of these sites (W01243 – Figure 8) the ReMi method resolved a low velocity zone (LVZ) that the refraction method cannot image.

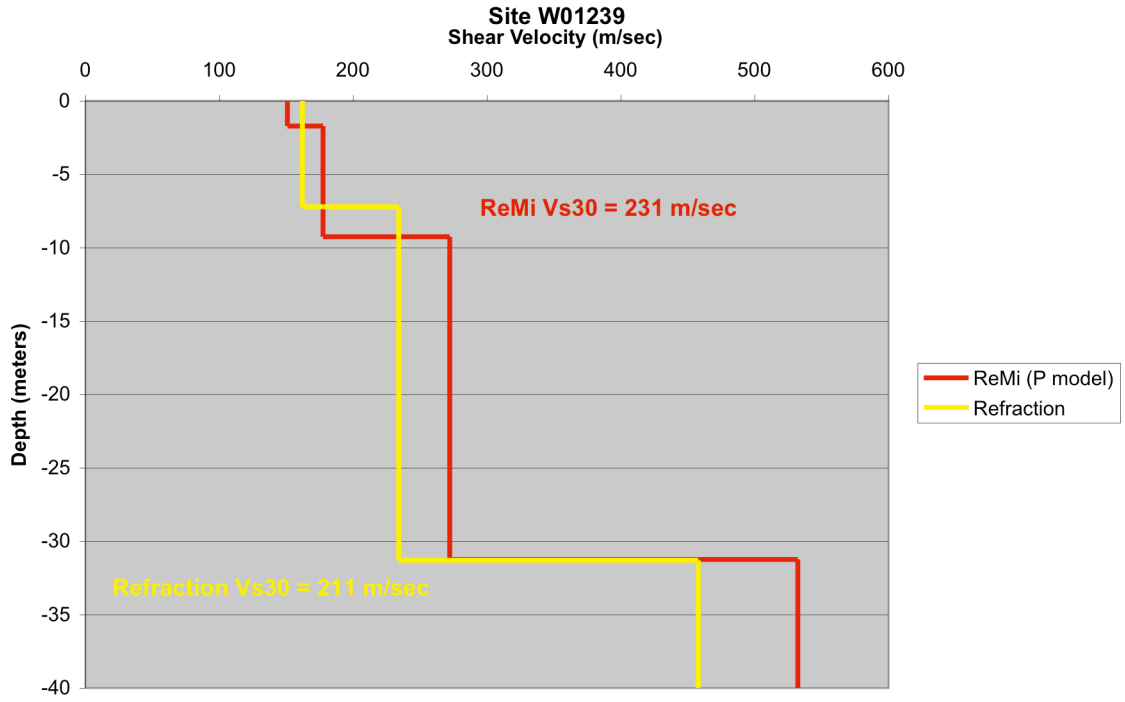

Figure 7: Comparison of shear wave refraction & ReMi V_S structure at site W01239. Note that V_{S30} values agree within 10%.

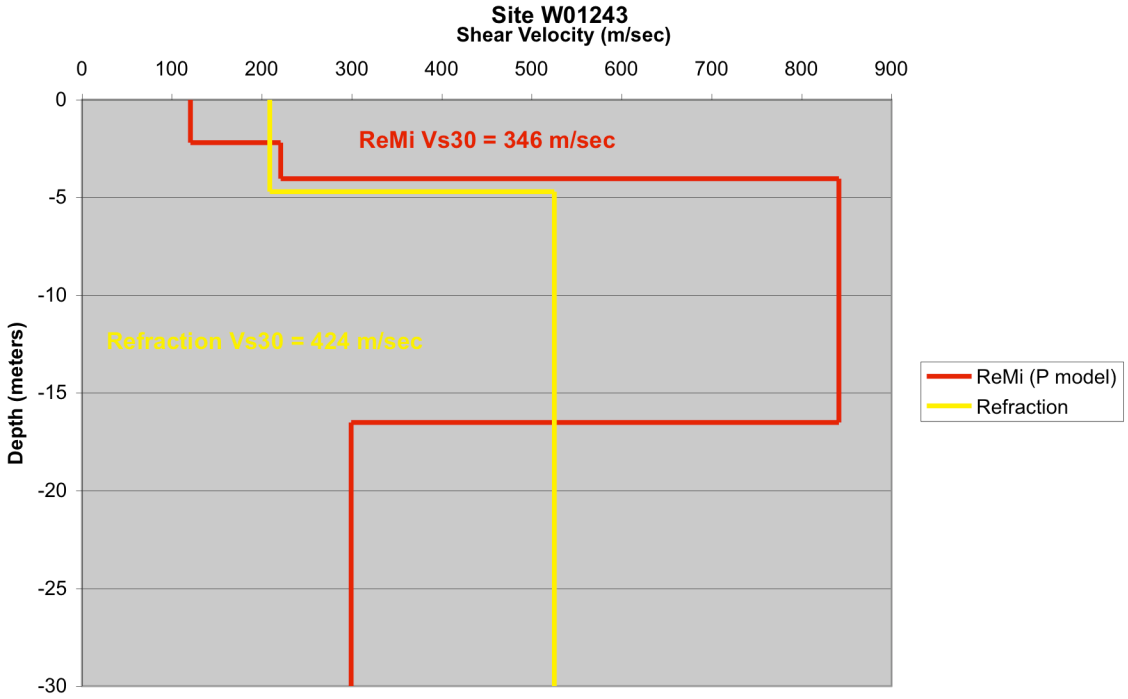

Figure 8: Comparison of shear wave refraction & ReMi V_S structure at site W01243. ReMi method resolves a LVZ at 16.5 meters and has a substantially smaller V_{S30}.

ReMi versus SCPT V_s Models

A major purpose of this work was to compare V_S structure derived from the surficial seismic methods to SCPT borehole data. Unfortunately most of the available SCPT tests are relatively shallow; only 5 go to depths greater than 20 meters (including W02104 which does not have a P-velocity model), 8 go between 10 and 20 meters, and the remaining 8 go less than 10 meters. In Figure 9 we compare ReMi and SCPT V_S structure at 4 sites where SCPT data exists below 20 meters; the other site is shown in Figure 4. While differing in detail, we find that the SCPT and ReMi velocity structures are similar and the estimated V_{S30} agree within 20% (within 10% for 4 sites).

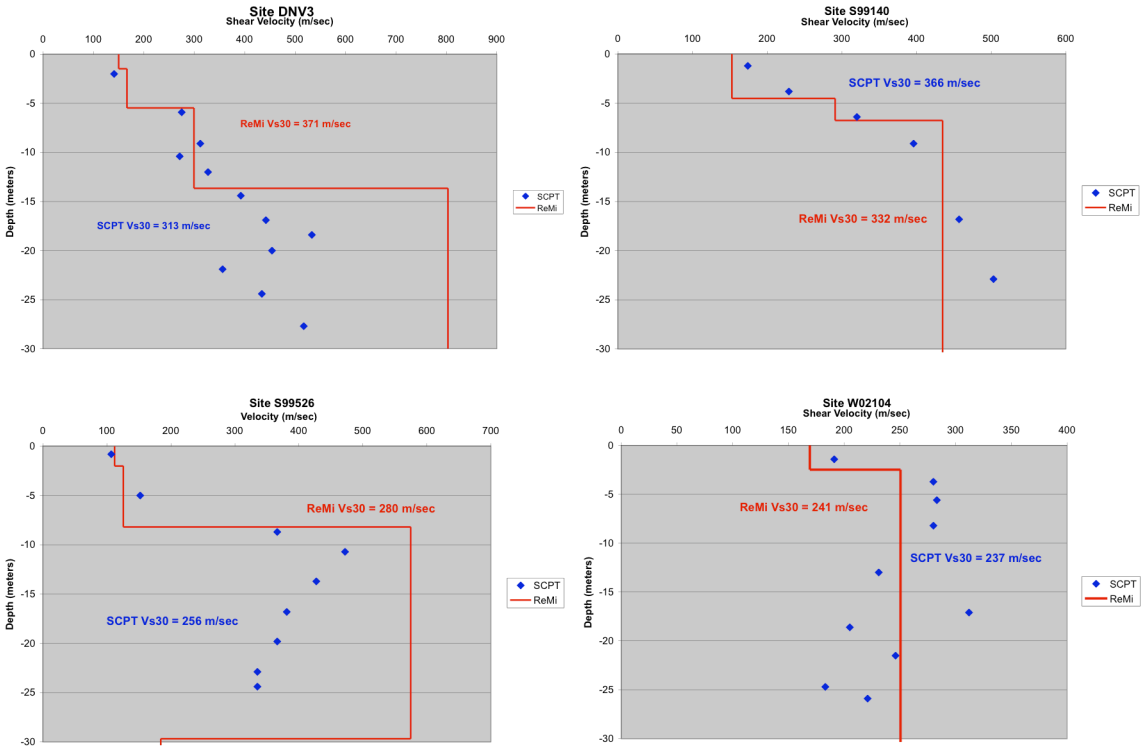

Figure 9: Comparison of SCPT & ReMi V_S structure at sites DNV3, S99140, S99526 and W02104. Note that at site W02104 we do not have a P-velocity model; therefore we used an average of the water table depths and P-velocity at water table from the 20 sites with a P-velocity model to constrain the ReMi V_S structure.

An overall comparison between SCPT and ReMi V_{S30} values is difficult because so few sites have SCPT values that go below 20 meters depth. In Figure 10 we attempt such a comparison by assuming the deepest SCPT V_S value extends to 30 meters depth. For 11 of 21 the sites this will underestimate V_{S30} (relative to the ReMi results) by more than 15%.

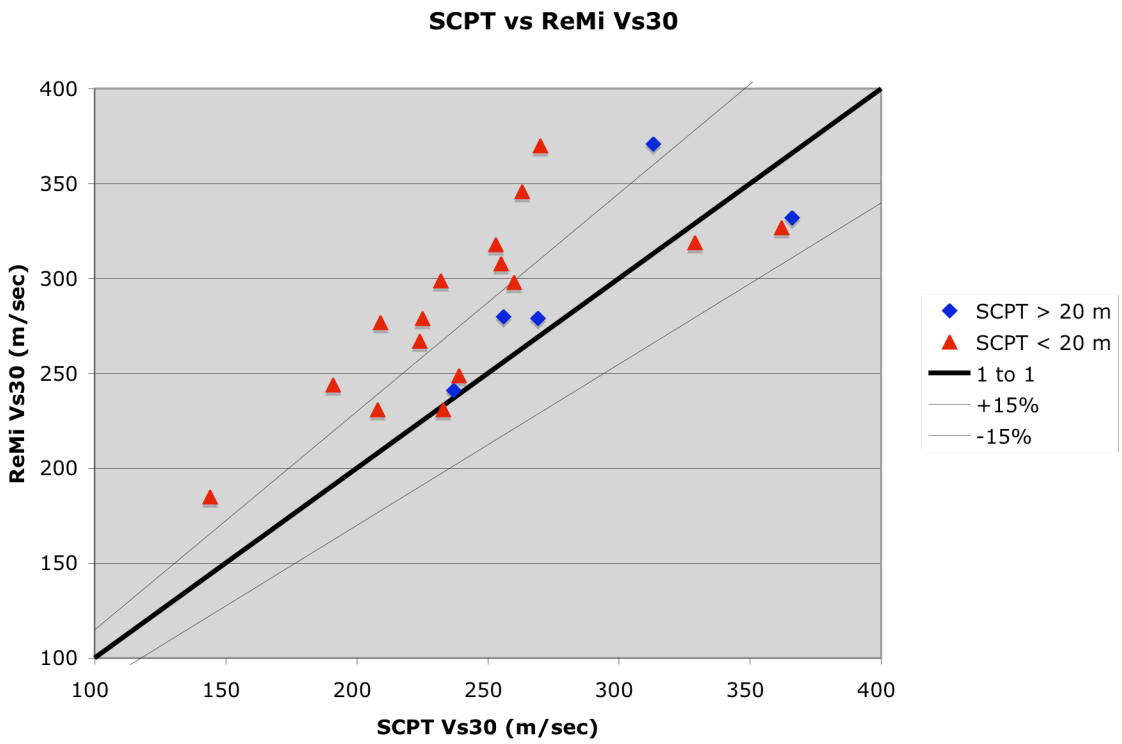

Figure 10: Comparison of SCPT & ReMi V_{S30} values at all 21 sites studied.

We also compare our ReMi V_{S30} and surficial geology, to see if there correlations between them that may be useful in microzonation studies. Figure 11 shows this comparison for the 21 sites studied. There is a tendency for V_{S30} to increase with increasing age of the surficial deposits, but there are too few sites in the youngest and oldest age categories to confirm this trend.

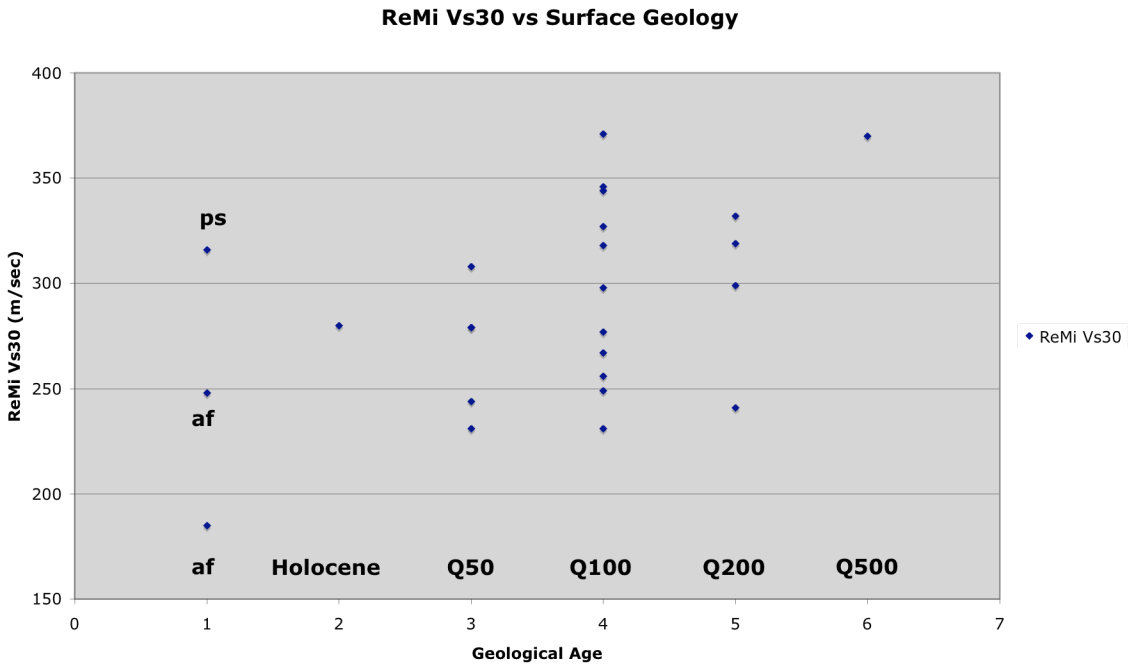

Figure 11: Comparison of ReMi V_{S30} and surficial geologic units. af (artificial fill) and ps (phosphate mining spoil) are strongly human modified sites, most other sites have some human disturbance in the upper few meters. Q50, etc., represent Quaternary surfaces with the numerical values being the approximate age in 1000's of years (e.g., Q100 = 100,000 years).

Data Products

As noted above, seismic data collected during this project can be accessed via the Charleston Seismic Hazard Analysis Consortium (CSHACe) WebGIS (http://maps.cofc.edu/website/cshacegis/viewer.htm). Additional funds were received during the course of this project to update and improve the CSHACe website and WebGIS. Databases used in this project, plus additional data useful for seismic hazard studies in the Charleston, South Carolina region, have been included in the WebGIS product. Additional databases, including earthquake catalog and newer SCPT databases will be included as time and funding permits. Table 5 lists the databases currently in the CSHACe WebGIS.

Table 5: Databases currently accessible via the CSHACe WebGIS. CofC = College of Charleston; SCDNR = South Carolina Department of Natural Resources, VTSO = Virginia Tech Seismological Observatory

Database	Brief Description	Source
anss_sites	Locations of ANSS strong motion stations	S. Jaume, CofC
basic_bedrock	State level bedrock geology	SCDNR
charl_Geology_dtl	Charleston region detailed geology	USGS
clip_maj_hwy	Major highways in Charleston County	Charleston County
counties	Boundaries of South Carolina counties	US Census Bureau
cpt_data_chapman	CPT sites in Charleston region with ground motion response estimates	M. Chapman, VTSO
dem_dtl	Charleston region digital elevation model	USGS
fema_q3_floodmap	FEMA floodmaps of Charleston County	FEMA
generalized_map	State level generalized geology	SCDNR
rectifycharleston_1885	1885 map of Charleston geo-rectified to modern street map	N. Levine, CofC
remi_sites_jaume	Locations of ReMi sites	S. Jaume, CofC
sc_boundary	Boundary of South Carolina	
scpt_data_chapman	SCPT sites in Charleston region with ground motion response estimates	M. Chapman, VTSO
spt_data_chapman	SPT sites in Charleston region with ground motion response estimates	M. Chapman, VTSO
statewidedem	Digital elevation model of South Carolina	SCDNR
surface_geol	South Carolina surficial geology	SCDNR

Publications Supported

Jaumé, S.C. (2008). Shallow shear wave structure in Charleston, South Carolina: a comparison of results from surficial seismic and borehole techniques, *to be submitted to the Bulletin of the Seismological Society of America*.

Jaumé, S.C. (2007). Shallow shear waves in Charleston, South Carolina: comparison of ambient noise and borehole techniques (abstract), Abstracts with Programs – Geol. Soc. Amer. **39**, pp.26.

Anderson, K.E., Jaumé, S.C., Andrus, R.D. and N. S. Levine (2006). Charleston Seismic Hazard Analysis Consortium (CSHACe): an urban hazards collaboration (abstract), Seis. Res. Lett. **77**, 96.

Brown, C.M., Jaumé, S.C. and S. L. Cooper (2006). Shear wave velocities from ambient seismic noise, Charleston, South Carolina (abstract), Seis. Res. Lett. **77**, 97.

Jaumé, S.C., Brown, C.M. and S.L. Cooper (2006). Shear wave structure in Charleston, South Carolina: initial comparison between SCPT, refraction and ambient noise techniques (abstract), Seis. Res. Lett. **77**, 96.

Acknowledgements

College of Charleston undergraduate students C. Brown, S. Cooper and K. Staggers participated in the collection of field seismic data. Students C. Brown, S. Cooper and R.

Kamaria helped process and interpret the seismic data. M. Chapman provided the SCPT database used in this work and personnel from S&ME, Inc. and WPC Engineering, Environmental and Construction Services helped with locating the SCPT sites.

References

Bakun, W. H., and M. G. Hopper (2004). Magnitudes and locations of the 1811-1812 New Madrid, Missouri and the 1886 Charleston, South Carolina earthquakes, Bull. Seism. Soc. Amer. **94**, 64-75.

Chapman, M. C., J. R. Martin, G. Olgun and B. Regmi (2003). Prediction and geographical information system (GIS) mapping of ground motions and site response in Charleston, SC and two neighboring counties: first phase development of a GIS for seismic hazard evaluation, final report, USGS Grant 00HQGR0036.

Frankel, A. D., Petersen, M. D., Mueller, C. S., Haller, K. M., Wheeler, R. L., Leyendecker, E. V., Wesson, R. L., Harmsen, S. C., Cramer, C. H., Perkins, D. M., and K. S. Rukstales (2002). Documentation for the 2002 update of the national seismic hazard maps, U.S.G.S. Open-File Rpt. 02-240, 33 pp.

Johnston, A. C. (1996). Seismic moment assessment of earthquakes in stable continental regions, III. New Madrid 1811-1812, Charleston 1886, and Lisbon 1755, Geophys. J. Int. **126**, 314-344.

Louie, J. N. (2001). Faster, better shear-wave velocity to 100 meters depth from refraction microtremor arrays, Bull. Seism. Soc. Amer. **91**, 347-364.

Odum, J. K., R. A. Williams, W. J. Stephenson and D. M. Worley (2003). Near surface S-wave and P-wave seismic velocities of primary geological formations on the Piedmont and Atlantic coastal plain of South Carolina, USA, USGS Open File Report **03-343**.

Robinson, A., and P. Talwani (1983). Building damage at Charleston, South Carolina, associated with the 1868 earthquake, Bull. Seism. Soc. Amer. **73**, 633-652.

Saito, M. (1979). Computations of reflectivity and surface wave dispersion curves for a layered media. I. Sound wave and SH wave, Butsuri-Tanko **32**, 15-26.

Talwani, P., and W. T. Schaeffer (2001). Recurrence rates of large earthquakes in the South Carolina coastal plain based on paleoliquefaction data, J. Geophys. Res. **106**, 6621-6642.